Characterization of retention and separation mechanisms with Pirkle-type enantioselective stationary phases in supercritical fluid chromatography

Caroline West, Syame Khater

HAL Id: hal-03490206
https://hal.science/hal-03490206

Submitted on 23 Jun 2022

1   **Characterization of retention and separation mechanisms with**

2   **Pirkle-type enantioselective stationary phases in supercritical fluid**

3   **chromatography**

4

5

6   Caroline West *[1], Syame Khater[1]

7   1. Univ Orleans, CNRS, Institut de Chimie Organique et Analytique (ICOA), UMR 7311,

8   B.P. 6759, rue de Chartres, F-45067 Orléans cedex 2, France.

9

10

11   Corresponding author:

12   Tel.: (+33)238 494 778

13   caroline.west@univ-orleans.fr

14

15

16

Abstract

17

18

19

20 In the present study, we characterize a famous Pirkle-type enantioselective stationary phase
21 ((R,R)-Whelk-O1 from Regis Technologies) and an equivalent enantiomeric phase (ReproSil
22 Chiral-NR from Dr. Maisch) in supercritical fluid chromatography (SFC) with carbon dioxide –
23 methanol (90:10 v/v) mobile phase. First, the interactions contributing to retention are
24 evaluated with a modified version of the solvation parameter model, comprising five Abraham
25 descriptors (E, S, A, B, V), two additional descriptors to take account of molecular shape
26 (flexibility F and globularity G), and two additional descriptors to take account of interactions
27 with ionizable species (D$^-$ and D$^+$). Linear solvation energy relationships (LSER) are
28 established based on the retention of 212 achiral analytes. As expected, π-π interactions are
29 the most significant to explain retention, while dipole-dipole, hydrogen bonding and ionic
30 interactions with cationic species are of secondary importance.
31 Secondly, the contributions of interactions to enantioseparations are discussed, based on the
32 analysis of 79 racemates. Discriminant analyses (DA) were computed to gain some insight
33 on retention mechanisms. The set of racemates is first divided between racemates eluted
34 earlier than expected based on the LSER models, and those eluted later than expected.
35 Small spherical molecules are more retained than expected, as they may better fit inside the
36 cleft of the chiral selector. They are also most frequently resolved, probably for the same
37 reason. Among the molecules that are less retained than expected, which are rather large
38 and/or non-spherical, other features are favourable to enantiorecognition: π-electrons,
39 dipoles and electron-donating properties. Contrary to the observations on other sorts of chiral
40 selectors, flexibility was found to have no contribution on the enantiorecognition process.
41

42

43

44

45 **Keywords:** chiral stationary phases; discriminant analysis; enantioseparation mechanisms;
46 Pirkle-type phases; solvation parameter model; supercritical fluid chromatography.

47

48

49

1. Introduction

Brush-type chiral stationary phases (CSPs) [1] were among the first chiral selectors purposely designed for liquid-phase chromatographic resolution of enantiomers. Previously, naturally occurring chiral selectors like proteins [2] or amino acids (particularly for ligand-exchange chromatography [3]) had been immobilized on silica supporting phases for use in enantioselective liquid chromatography. Brush-type CSPs with charge-neutral synthetic selectors were initially developed by William H. Pirkle and co-workers from the end of the 1970s [4,5], which is why these phases are often named "Pirkle-type". The idea behind the ligands proposed was to offer three points of interaction that would comply with the "three-point attachment model" initially proposed by Easson and Stedman for protein binding [6], and later adapted for enantioselective chromatography by Dalgliesh [7]. Although not entirely accurate in describing the enantioseparation process, it is still convenient to design such chiral selectors based on this model. As appears with the example in Figure 1, the chiral ligands are designed to have three (or more) different interaction points. However, what does not appear on this figure is that the bulky ligands also have a well-defined, rather rigid spatial arrangement [8–10], with the tetrahydrophenanthrene ring and the dinitrobenzyl ring being positioned in an orthogonal fashion, thereby forming a cleft. The dinitrobenzyl group appears to be the only one with some conformational flexibility, somewhat rotating to bind the analytes inside or outside the cleft [8,10]. As a result, chiral discrimination is favoured when steric fit occurs, that is to say when the enantiomers have the adequate size, shape and three-dimensional organization of the interacting groups to fit in the chiral cleft of the ligand [5,11]. Three-dimensional structures have been shown in the past, based on crystallographic measurements [11] or based on molecular modelling [8–10].

Compared to other CSPs that are now frequently used like polysaccharides [12–14], macrocyclic glycopeptides [15–17] or protein-based phases [2], one advantage of such brush-type phases is that the ligand has a controlled chiral configuration, and an enantiomeric form may exist with the opposite configuration. For instance, the most famous Whelk-O1 stationary phase designed by Pirkle and Welch [18] can be found in (R,R) configuration (as in Figure 1) or in (S,S) configuration, thereby offering the possibility to control the elution order of enantiomers by choosing one chiral selector or its enantiomeric form. Indeed, when the aim of the chiral separation is to measure an enantiomeric excess, the minor enantiomer should preferably elute first to avoid being masked by the tailing peak of the major enantiomer. On the contrary, when purification is desired, the preferred enantiomer (whichever its proportion) should elute first because the first peak purified is usually obtained with a higher purity than the second. Indeed, although their loadability is not

86   as high as that of polysaccharide CSPs, it is still higher than the loadability of CSPs based on

87   proteins, cyclodextrins and macrocyclic glycopeptides [19], making Pirkle-type CSPs useful

88   for preparative purposes. Stereoismer identification and measuring extreme enantiomeric

89   excess values (>99%) can be enabled by the possibility to reverse the stereoisomers elution

90   order with chiral selectors of opposite configuration, as was demonstrated with the "Inverted

91   Chirality Columns Approach" proposed by Gasparrini and co-workers [20–22].

92   Following the current trend of reducing particle size, the most recent version of Whelk-O1 for

93   analytical-scale separations is available on sub-2 μm fully porous particles and has

94   demonstrated improved efficiencies, as could be expected [23,24].

95   While Pirkle-type stationary phases were mostly employed in high-performance liquid

96   chromatography (HPLC), they are also useful in supercritical fluid chromatography (SFC),

97   where they are usually found to offer complementary capabilities for enantioselectivity to the

98   most employed polysaccharide CSPs [25]. In this field, the Whelk-O1 phase appears as the

99   most widely distributed brush-type phase. Modern SFC is essentially based on the use of

100   pressurized carbon dioxide as the principal component of the mobile phase, together with a

101   co-solvent (most often a short-chain alcohol) [26,27]. Thanks to several interesting attributes

102   of carbon dioxide (low toxicity, no safety issues, low price) and the inherent advantages of

103   the technique (low-viscosity fluid and high diffusivities providing high efficiencies even at high

104   flow rates, low amount of waste especially after preparative separations), SFC has long been

105   a favourite to achieve enantioseparations [28,29], usually offering higher resolution per unit

106   time than enantioselective HPLC, thanks to high efficiency and high flow rate [30,31].

107   In previous works, we have proposed a chemometrics strategy to improve understanding of

108   SFC enantioseparation mechanisms based on the use of linear solvation energy

109   relationships (LSER) and discriminant analyses (DA) [32,33]. First, we developed a modified

110   version of the solvation parameter model, comprising five Abraham descriptors (E, S, A, B,

111   V) and four additional descriptors that were introduced to bring complementary information

112   related to (i) analyte shape features of flexibility (F) and sphericity (or globularity, G) and (ii)

113   ionic interaction capability through anionic (D^-) and cationic (D^+) analyte properties. With this

114   model, we have previously examined polysaccharide CSPs [34,35], macrocyclic

115   glycopeptide CSPs [36,37] and *Cinchona*-based brush-type CSPs [38], all in SFC

116   conditions. In the present paper, this modified solvation parameter model is employed to

117   characterize the (R,R)-Whelk-O1 enantioselective stationary phase in supercritical fluid

118   chromatography based on the analysis of 212 achiral analytes. A similar phase from a

119   different manufacturer (ReproSil Chiral-NR), carrying the (S,S) enantiomeric ligand from

120   (R,R)-Whelk-O1 was included for comparison purposes, as we had observed in the past that

121   supposedly identical enantioselective stationary phases provided by different manufacturers

122   could sometimes be significantly different [39].

123   Secondly, we have also demonstrated earlier that discriminant analysis (DA) was a useful

124   tool to unravel the contributions of analyte features to enantiorecognition [34–36]. Based on

125   the analysis of 79 chiral analytes, the structural features contributing to favourable

126   enantiorecognition of (R,R)Whelk-O1 in SFC will be discussed.

127

128

129   ## 3. Material and methods

130

131   ### 3.1. Stationary phases

132

133   The stationary phases used in this study are commercially available: (R,R)-Whelk-O1 from

134   Regis Technologies was packed in 150 x 4.6 mm column, with fully porous 5 µm silica

135   particles, and ReproSil Chiral-NR (bonded with the (S,S) ligand) from Dr. Maisch was

136   packed 250 x 4.6 mm column, with fully porous 8 µm silica particles.

137

138   ### 3.2. Chemicals

139

140   The solvent used was HPLC-grade methanol (MeOH) provided by VWR (Fontenay-sous-

141   Bois, France). Carbon dioxide of industrial grade 99.5% was provided by Air Liquide

142   (France). 212 achiral test compounds (Table S1 in supplementary information) were obtained

143   from a range of suppliers and were used to evaluate the contributions of molecular features

144   to retention through LSER. 79 chiral racemic test compounds (Table S2 in supplementary

145   information) were used to evaluate the contributions of molecular features to

146   enantiorecognition through DA.

147

148

149   ### 3.3. Chromatographic system and conditions

150

151   Chromatographic separations were carried out using equipment manufactured by Jasco

152   (Tokyo, Japan). Two model 980-PU pumps were used, one for carbon dioxide and a second

153   for the modifier. Control of the mobile phase composition was performed by the modifier

154   pump. The pump head used for pumping the carbon dioxide was cooled to −5 °C by a

155   cryostat (Julabo F10c, Seelbach, Germany). When the two solvents (methanol and CO_2)

156   were mixed, the fluid was introduced into a dynamic mixing chamber PU 4046 (Pye Unicam,

157 Cambridge, UK) connected to a pulsation damper (Sedere, Orleans, France). The columns

158 were thermostated by an oven (Jetstream 2 Plus, Hewlett-Packard, Palo Alto, USA),

159 regulated by a cryostat (Haake D8 GH, Karlsruhe, Germany). The detector was a Gilson UV

160 151 detector (provided by Waters, Milford, MA) equipped with a pressure-resistant cell. After

161 the detector, the outlet column pressure was controlled by a Jasco BP-2080 Plus pressure

162 regulator. The outlet regulator tube (internal diameter 0.25 mm) was heated to 60 °C to avoid

163 ice formation during the CO_2 depressurization. The UV detection wavelength was 210 nm.

164 Chromatograms were recorded using the Azur software (Datalys, France).

165 The mobile phase used in this study is always CO_2-MeOH 90:10 (v/v) without any additive.

166 Flow rate was 3 mL min^{-1}. The oven temperature was set at 25°C and the outlet pressure

167 was maintained at 15 MPa. Strictly speaking, the fluid is thus not supercritical but could be

168 called subcritical. No distinction will be made in the following.

169

170 ### 3.4. Data analysis

171

172 The Abraham solute descriptors (E, S, A, B, V) used for LSERs with Eq. (1) were extracted

173 from an in-house database established from all available literature on the solvation

174 parameter model (Tables S1 and S2). The two additional descriptors for charges (D$^-$ and D$^+$)

175 were calculated based on aqueous pK_a values determined with Chemicalize program and

176 apparent pH 5. See previous works for detailed description [40]. The additional descriptors

177 for flexibility (F) and globularity (G) were computed as previously described [32,33].

178 Multiple linear regressions (MLR) and discriminant analysis (DA) were performed using

179 XLStat 19.03.44850 software (Addinsoft, New York, NY). The quality of the MLR fits was

180 estimated using the adjusted determination coefficient (R^2), standard error in the estimate

181 (*SE*) and Fisher *F* statistic. The statistical significance of individual coefficients was evaluated

182 with the 95% confidence intervals.

183 The quality of DA was estimated based on ROC (receiver operating characteristics) curves

184 and confusion matrices (see Figure S1 in supplementary information).

185

186 ## 4. Results and discussion

187

188 The stationary phases examined in this paper bear the same chiral selector (in two

189 enantiomeric forms), presented in Figure 1. The ligand can be fragmented into three

190 sections: two aromatic rings arranged in a perpendicular orientation, with one being π-donor

191 (the tetrahydrophenanthren ring) and the other one being both a π-acceptor, a dipole-dipole

192   interaction site and a hydrogen bond acceptor site (the 3,5-dinitrobenzoyl ring); between

193   them is an amide function acting as a hydrogen-bond system, which can contribute to

194   hydrogen bonding both as a proton donor (-NH- group) and as a proton acceptor (C=O

195   group). This stationary phase is one of those of which the recognition mechanism has been

196   described with most details [4] and is supposedly one of the easiest to explain (unlike the

197   most complex CSPs based on polysaccharide of macrocyclic glycopeptides). Many of the

198   molecular modelling studies to date were down with the chiral selector placed in a supposed

199   "gas state" (not considering possible mobile phase components) [41], or sometimes in a

200   "liquid state" (considering solvent molecules) [9], and always compared the computational

201   results to liquid chromatography experimental data. In papers from Cann and co-workers

202   relating docking studies [9,10], four interaction modes (M1-M4) were observed to occur

203   between the analytes and the chiral selector. The latter was mostly in one, energetically

204   more stable conformation, but could adopt a slightly different conformation for one interaction

205   mode (M1 "side-of-cleft binding"), with the dinitrophenyl group rotating in a perpendicular

206   position. It was also shown that predicting the outcome of a separation on this stationary

207   phase was possible, with rather high success rate of the prediction [42], which is another

208   indication of a well-defined enantiorecognition process. Comparison to the knowledge

209   previously acquired with molecular modelling and liquid chromatography, to our results,

210   based on a statistical model and observations done in pressurized carbon dioxide –

211   methanol mobile phase, was also of interest in this study.

212   The sets of achiral and chiral probe analytes were previously designed for the

213   characterization of polysaccharide CSPs. It is worth mentioning that it is still adequate to

214   characterize these brush-type CSPs as appears from Figure 2.

215   First, the retention data of the achiral analytes (Table S1) are adequately scattered in a wide

216   retention space with log k values ranging from -1 to +2 (Figure 2a). Besides, the retention

217   data between the two columns were highly correlated (R^2 = 0.97), but the slope of the

218   correlation line was significantly inferior to 1 (0.80) indicating that the two columns have

219   *homeoenergetic* behaviour, according to the definition proposed by Horváth and co-workers

220   [43], and suggesting similar physico-chemical basis for retention on the two columns. The κ-κ

221   plot (log k vs. log k) can be observed in Figure S2 provided in supplementary information.

222   The observed slope inferior to 1 may simply result from the different silica particles employed

223   to support the chiral selector. Full information on the silica (pore size, specific surface area)

224   and bonding density was not available, but the two CSPs had different particle size (5 and 8

225   μm).

226   Secondly, the separation data measured for the analytes in Table S2 are also adequately

227   scattered with log α values ranging from 0 to 0.4 (Figure 2b) and about 60% showing α

228   values >1. For the purpose of identifying the structural features contributing to

7

229 enantiorecognition, it is important that the probe set comprises both resolved and non-
230 resolved enantiomers.

231

232 **_4.1. Interactions contributing to retention_**

233

234 The LSER equation employed in this work was previously described [37]:

235 $$\log k = c + eE + sS + aA + bB + vV + d^-D^- + d^+D^+ + fF + gG \qquad (1)$$

236

237 Briefly, the capital letters are molecular descriptors: E is related to the presence of π and n
238 electrons, S is related to the presence of dipoles, A is related to proton-donor capability, B is
239 related to electron-donor capability, V is the molecular volume, D^- is the total negative
240 charge, D^+ is the total positive charge, F qualifies the molecule flexibility and G is the
241 molecule sphericity. The small case letters are the system constants obtained from multiple
242 linear regression of retention data (log k values) for a large set of analytes with known
243 descriptor values. They quantify the relative contribution of interactions to the retention
244 mechanism.

245

246 The results of LSER characterization are presented in Figure 3 (normalized coefficients), with
247 complete data and statistics available in Table 1. The statistics were reasonably good, with
248 R^2_{adj} values of about 0.85 and standard deviation in the estimate of 0.28 and 0.14 for Whelk-
249 O1 and ReproSil Chiral-NR respectively. These results are clearly not as good as is usually
250 observed when the solvation parameter model is applied for achiral separations, whatever
251 the chromatographic mode, but considering the complexity of the system used here, they
252 should be good enough to interpret the contributions of interactions to retention. The two
253 columns yielded identical models as no significant difference can be observed (considering
254 standard error bars). This is in accordance with the previous observation of high correlation
255 of the retention data (Figure S2).
256 A first observation is that the e term, reflecting interactions associated to the presence of π
257 and n electrons in the analytes, is by far the most significant one to contribute to retention.
258 This was naturally expected, judging from the two aromatic groups (dinitrobenzyl and
259 tetrahydrophenanthryl) in the chiral selector. Halogen bond [44], occurring between halogen
260 atoms of some probe analytes and the nitrogen and oxygen atoms or π-donor system of the
261 chiral selector may also be included in this e term. Typically, retention increase is observed
262 when moving from chloride to bromide and iodide. For instance, this can be observed with
263 halogenobenzenes (analytes #87 to #89 in Table S1) and halogenonaphthalenes (analytes
264 #96 to #98).

8

265 Next to the *e* term, hydrogen bonding interactions with proton donors (*a* term) and acceptors
266 (*b* term) are the most significant, and are related to the presence of the amide function in the
267 chiral selector, which can interact both with proton donors (*a* term) and proton acceptors (*b*
268 term), but also to the presence of nitro groups that can interact with proton donors [8–
269 10,45].The influence of hydrogen bonding can be observed for instance in the increased
270 retention observed when increasing the number of hydroxyl groups in the analyte, as for
271 phenol, resorcinol and phloroglucinol (analytes #103, 108 and 111 in Table S1), or for any
272 pair of analytes differing from one hydroxyl group (many possible pairs in Table S1).
273 Of slightly inferior significance are the dipole-dipole interactions (*s* term) related to the amide
274 and nitro functions, and the interactions with cationic species (d^+ term), possibly due to non-
275 bonded silanol groups at the surface of the silica supporting phase. The latter would also
276 cause some repulsion to anionic species, as appears from the negative d^- term. Another
277 possible contribution to the retention of ionic analytes is through the aromatic groups of the
278 chiral selector. Firstly, the nitro functions carry partial negative charges on the oxygen atoms,
279 which could also be responsible for the attraction of cationic analytes and repulsion of
280 anionic analytes. Secondly, the tetrahydrophenanthrene ring is a π-donor system, which
281 could also interact with electron-deficient cationic analytes and be responsible for the positive
282 d^+ term. It is also worth mentioning that the d^-/d^+ terms are not significantly different between
283 the two stationary phases, suggesting that silanol accessibility and/or ligand bonding density
284 should be comparable between the two phases.
285 From these models, analyte size (described by the V descriptor) appears to have no
286 influence on analyte retention. However, the analyte shape described by the G descriptor is
287 significant: spherical molecules (large G values) must be somewhat sterically excluded from
288 the stationary phase, as opposed to flat and/or linear molecules (small G values). Significant
289 examples can be observed with polynuclear aromatic hydrocarbons. For instance, *p*-
290 terphenyl (analyte #180 in Table S1), a rod-like molecule, is more retained than *o*-terphenyl
291 (analyte #179) which is more spherical, as indicated by a larger G value. These observations
292 may be somewhat contradicted because there is some inter-correlation between the V and G
293 terms (R^2 = -0.77). When retaining only the five Abraham descriptors in the model
294 calculation, the *v* term is significant and positive, although small, indicating that the retention
295 of large molecules is favoured by (i) interaction with the aromatic rings (dispersive or CH-π
296 interactions), or (ii) to a lesser extent, dispersive interactions with the alkyl spacer arm linking
297 the chiral selector to the silica surface. For instance, increasing alkyl chain length, which is
298 inducing increasing V values while all other molecular descriptors remain virtually constant, is
299 causing a slight increase in retention. Typically, this can be observed in the alkylbenzene
300 series (analytes #2 to #15 in Table S1), phenylalcohol series (analytes #70 to #72),

301   alkylphenone series (analytes #80 to #82), alkylbenzoate series (analytes #152 to #155),

302   dialkylphthalate series (analytes #156 to #159), and parabens (analytes #160 to #163).

303   Finally, flexibility (described by F descriptor) has no influence on retention neither. It was

304   never observed to have an influence on retention on the other CSPs previously tested [34–

305   38], but is retained in the model for its possible contribution to enantiorecognition.

306

307

308   **4.2. Enantioseparation capabilities**

309

310   Because the two stationary phases were observed to be most similar in their retention and

311   separation behaviour, only the results for the Whelk-O1 phase will be detailed in the

312   following.

313

314   In previous works, we have had several occasions to demonstrate a strategy to explain

315   enantioseparation mechanisms with discriminant analyses (DA). Discriminant analysis is a

316   supervised method: the samples (in the present case the racemates) are first classified into

317   two sets of classes (i) based on experimental retention compared to predicted retention

318   (eluted earlier *vs*. later than predicted), or (ii) based on enantioselectivity ($\alpha = 1$ *vs*. $\alpha > 1$).

319   The first set of DA classes is based on experimental retention factors measured for the two

320   enantiomers and comparing these experimental values to the retention factor predicted by

321   Eq. (1), with the models calculated above based on the retention of achiral analytes (Table

322   1). Because the descriptors are identical for the two enantiomers, there is only one predicted

323   retention factor for each racemate. Usually, both enantiomers appear to be either less

324   retained than predicted, or more retained than predicted, with one of them being close to the

325   predicted value. In rare cases, the first eluted enantiomer is less retained than predicted

326   while the second eluted enantiomer is more retained than predicted. We then have divided

327   the whole set of racemates (see DA classes in Table S2) into two classes: the "early-eluting

328   racemates" and the "late-eluting racemates". Discriminant analysis applied to the whole set

329   of racemates, using their molecular descriptors as variables and the two classes thus defined

330   is yielding Figure 4a for Whelk-O1. The AUC (area under the ROC curve, which can be

331   observed in supplementary information Figure S1) was 0.829, indicating that the

332   classification obtained is statistically significant. Because there are only two classes, a single

333   axis is sufficient to represent 100% of the variance. On Figure 4a, the structural features that

334   point to the left of the figure have larger descriptor values in the racemates eluting earlier

335   than predicted, while the structural features that point to the right of the figure have larger

336   descriptor values in the racemates eluting later than predicted.

337   The size and shape features are all significant and can be explained as follows: the late-

338   eluting racemates are mostly small (molecular volume V is pointing to the left) and spherical

339   (globularity G is pointing to the right).The chiral ligand in these stationary phases is known to

340   form a semi-rigid cleft [8]. A large and flat or rod-like molecule (with small sphericity) is

341   unlikely to fit in the chiral cleft but may still be retained (and even resolved) through

342   interactions outside the cleft [46]. For instance, docking studies from Zhao and co-workers

343   [9,10] and from Roussel group [8] showed how the dinitrobenzyl ring could rotate to interact

344   with an analyte that would mostly remain outside the cleft. On the contrary, a small spherical

345   molecule is likely to better fit the walls of the chiral cleft and interact favourably with the

346   different groups of the ligand, favouring stronger retention. This hypothesis is also supported

347   by the observation that nearly all late-eluting racemates (25% of the complete set) showed

348   some enantiorecognition ($\alpha > 1$). In other words, when the enantiomers were favourably

349   included in the chiral cleft, some resolution occurred nearly systematically (19 cases out of

350   20) for this probe set. Metoprolol was the sole exception in this group. The "early-eluting"

351   racemates, supposedly not included in the chiral cleft, showed much lower success rates

352   with about 50% enantiodiscrimination observed.

353   We may also note that most acidic species, bearing some anionic charge in the present

354   operating conditions, also belong to this class of late-eluting racemates (D^- is pointing to the

355   right of the figure). This may be surprising since there are no ion-exchange interaction site

356   bearing a permanent charge in this stationary phase. There are however possible residual

357   silanol groups at the silica surface and the two aromatic groups of the chiral selector, which

358   are electron-rich (tetrahydrophenanthrene) and electron-deficient (dinitrobenzene). Residual

359   silanol groups should exert ionic repulsion to anionic analytes, as suggested from the LSER

360   models (negative d^- term). Repulsive interactions with the supporting phase may however be

361   favourable to interaction with the bonded chiral selector, as the analytes would be

362   preferentially retained on the chiral selector rather than penetrating deeper in the stationary

363   phase, thereby promoting enantioseparation. It was also shown [47] in previous molecular

364   modelling studies on Whelk-O1 that non-enantiospecific interactions could influence the way

365   the analytes were interacting with the chiral selector, thereby influencing the

366   enantiorecognition process. In addition, a negatively charged analyte and the π-accceptor

367   dinitrobenzyl ring of the chiral ligand may interact through anion-π interaction [48]. Such

368   interaction may be favoured by the relative flexibility of the dinitrobenzyl ring, which was

369   observed to adapt its torsion angle to favour analyte binding [8,10]. Further molecular

370   modelling studies would be necessary to support any of these hypotheses.

371

372   The second set of DA classes examined is based on the enantioselectivity. Any racemate

373   where some enantioseparation is observed ($\alpha > 1$) is classified as "separated" while $\alpha = 1$

374   would be classified as "non-separated". Processing the whole data set in one discriminant

375   analysis is possible and is yielding reasonably good statistics in this case (AUC = 0.782, see

376   supplementary information Figure S1). The result can be observed in Figure 4b. However, as

377   we have had occasions to demonstrate in the past [34,35], it is beneficial to use the above

378   early/late-eluting classifiers prior to the DA calculation, because different groups of analytes

379   may be resolved for different reasons. As mentioned above, all (but one) racemates eluting

380   later than predicted were "separated", thus no DA can be computed specifically for this group

381   as a sufficient number of negative cases are required to obtained statistically meaningful

382   results. The group of early-eluting racemates however was still large, comprising 59

383   racemates among which 30 were "not separated" and 29 were "separated". This is a

384   reasonably large and balanced data set to compute a DA, as the number of analytes is nealy

385   equal in each class. The result was statistically significant (AUC = 0.775, see Figure S1 in

386   supplementary information) and presented in Figure 4c. From this figure, we can note that,

387   when the racemates were early-eluting, even if they were mostly large (V pointing to the

388   right) and flat (or rod-like, G pointing to the left) as was defined in the early/late-eluting DA,

389   they could still be separated if they had π electrons to interact with the aromatic rings of the

390   chiral selector (E pointing to the right), dipoles to interact with the nitro groups or amide

391   group of the chiral selector (S pointing to the right) and electron-donating capability to form

392   hydrogen bonds with the –NH- group in the amide function (B pointing to the right). The

393   significant contribution of E, S, and B for this group is consistent with previous observations

394   [9,10], where molecular modelling indicated that many of the less retained analytes were

395   interacting with the chiral selector through the aromatic groups and through hydrogen

396   bonding with the amide proton. Other features (proton-donor capability A, presence of

397   negative or positive charges D^- and D^+ and flexibility F) were non-significant to explain the

398   differences between the two classes. This does not mean that they do not contribute to any

399   interactions but only that they were not sufficiently different between the two classes. For

400   instance, proton-donors (*a* term) and cationic species (*d⁺* term) were retained (according to

401   LSER model in Figure 3) but they were present equally in both racemate classes

402   ("separated" and "non-separated"). As a result the A term and D^+ term are both close to zero

403   in the discriminant analysis (Figure 4c). The non-discriminant contribution of A term is

404   consistent with the observed orientation of the carbonyl group towards the exterior of the

405   chiral cleft [5], and is also consistent with previous molecular modelling studies, where

406   hydrogen bonding between an analyte proton and the carbonyl or nitro functions of the chiral

407   selector were observed to be much less frequent than the hydrogen bonding to the amide

408   proton [8–10]. The interactions with cationic species could result from the presence of non-

409   bonded silanol groups, which should also be non-enantioselective, or from interactions with

410   the two aromatic groups (tetrahydrophenantrenyl and dinitrobenzyl), as mentioned in the

description of retention models. Most anionic species were included in the late-eluting class thus this feature (D^-) could not be evaluated in the early-eluting class where most analytes had zero D^- value.

Finally, it is interesting to note that flexibility (F term) was non-discriminant. This is rather surprising because flexibility was found to be very significant as an unfavourable feature to enantiorecognition with other CSPs previously characterized, particularly with polysaccharide CSPs and *Cinchona*-based brush-type CSPs [38]. Flexibility is usually deleterious to enantiorecognition because flexible molecules have more conformers, that make the two enantiomers less easily discriminated. Also, as pointed out by Lämmerhofer [49], rigid molecules require less interactions to achieve enantioselectivity as they meet the geometrical requirements easier than flexible molecules. From the discriminant analyses presented here, this is clearly not an issue on these Pirkle-type CSPs. The supposedly negative effects of flexibility may be contradicted by a positive dynamic fit, whereby the interactions between the flexible analytes and the ligand are favoured by conformational adaptation. It is possible that this flexible adaptation of the analyte would be facilitated by the semi-rigid structure of the chiral selector in this Pirkle-type phase, compared to more flexible CSPs (like those based on polysaccharides).

Considering all information from the retention models and discriminant analyses, Figure 5 provides another look at the retention and separation data, in conjunction with structural features. Figure 5 is plotting log α between the two enantiomers versus log k of the first eluted enantiomer. Each point thus represents one racemate, while the bubble size is reflecting one structural feature. For instance, π-electrons (E), dipoles (S), sphericity (G) and cationic charges (D^+) are represented. On the top figures, it appears that the smallest values of E and S (small bubbles) are associated to small retention factors (in accordance with the retention models in Figure 3) and small separation factors (in accordance with Figure 4c). In the top right corner of these figures, the bigger bubbles indicate that the molecules that are π-electron-rich (large E values) and/or possess strong dipoles (large S values) have both strong retention and large enantioresolution. According to the observations in Figure 4, these may belong to the late-eluting class, if they are rather small (small V value), spherical (large G value) and possess negative charges (non-zero D^- value) through acidic functions. Typical examples are 2-phenylbutyric acid (analyte #2 in Table S2) and 2-phenylpropionic acid (#3). In addition, enantiomers with large E and/or S features and successful enantioseparation may also belong to the early-eluting class: Figure 4c indicates that favourable enantiorecognition in this case will also depend on the ability to form hydrogen bonds (B term) and the size and shape features, as big (large V value) and flat or rod-like (small G

448   value) molecules should be favoured. Typical examples are found in the group of β-blockers

449   Acebutolol (analyte #25 in Table S2), Atenolol (#27), Betaxolol (#28), Oxprenolol (#58),

450   Propranolol (#60) and Sotalol (#63). All of them have several heteroatoms with non-binding

451   electrons contributing to large S and B values, and they have long chains inducing both large

452   volume and rod-like shape. Another example is that of benzodiazepines Diazepam (#35),

453   Lorazepam (#49) and Oxazepam (#56) that are all rather large and flat.

454   However, strong E and S features are not sufficient to achieve enantioseparation, as can be

455   observed with some large bubbles at the bottom line of these figures, corresponding to zero

456   log α values. As mentioned above, no enantioresolution was principally observed in the

457   early-eluting racemates. Thus analytes with large E and S values eluting earlier than

458   expected may still be unresolved, particularly if they are rather small (small V value) and

459   spherical (large G value). Typical examples are found in the group of barbiturates like

460   Glutethimide (#42), Hexobarbital (#43), Secobarbital (#62) and Thiopental (#67): although

461   they have favourable electron and dipole features (E, S and B values), they are all rather

462   small and spherical and remain unresolved.

463   The bottom left figure in Figure 5 shows that spherical molecules (large G values) are mostly

464   distributed in low retention values (in accordance with Figure 3, indicating exclusion of

465   spherical molecules). However, small spherical molecules (case of "late-eluting racemates")

466   that are little retained are well separated as appears with positive values of log α on the left

467   of the figure. Again, this would be the case of 2-phenylbutyric and 2-phenylpropionic acids.

468   Non-spherical molecules (flat or rod-like) are more retained and can still be well separated

469   with favourable E, S and B features and a large molecular volume (case of "early-eluting

470   racemates" in Figure 4c). For instance, this is corresponding to the β-blockers and

471   benzodiazepines.

472   Finally, the case of cationic species is also interesting (bottom right figure). Cations (large D^+

473   values) are positively retained on this stationary phase (in accordance with Figure 3,

474   indicating favourable retention of cations), thus the large bubbles are mostly on the right side

475   of this figure. However, the presence of cationic charges was non-discriminant to explain

476   enantioseparation (Figure 4b and 4c), thus big bubbles can be found at all levels of α values.

477

478

479   **5. Conclusions**

480

481   Two Pirkle-type chiral stationary phases bearing the same (but enantiomeric) chiral selector

482   from two different manufacturers were characterized for their retention properties through

483   linear solvation energy relationships and for their enantioseparation properties through

484   discriminant analyses. The two stationary phases appeared to be most similar, with

485   *homeoenergetic* behaviour. π-π interactions were the most significant to explain retention,

486   followed by hydrogen bonding, dipole-dipole interactions and ionic interactions. Steric

487   exclusion was also significant to explain lack of retention for spherical molecules. The

488   racemates possessing favourable features for enantioseparation can be divided into two

489   groups: small spherical molecules that would well fit in the chiral cleft were nearly always

490   resolved, especially is they possessed negative charges. For large and flat or rod-like

491   molecules that are unlikely to fit so well in the chiral cleft, π-π interactions, dipole-dipole

492   interactions and electron-donating properties were most significant to achieve

493   enantioresolution. These observations are in accordance with chemical sense and previous

494   investigations on these chiral selectors.

495

496

501

References

[1] F. Gasparrini, D. Misiti, C. Villani, High-performance liquid chromatography chiral stationary phases based on low-molecular-mass selectors, J. Chromatogr. A. 906 (2001) 35–50. https://doi.org/10.1016/S0021-9673(00)00953-5.

[2] J. Haginaka, Protein-based chiral stationary phases for high-performance liquid chromatography enantioseparations, J. Chromatogr. A. 906 (2001) 253–273. https://doi.org/10.1016/S0021-9673(00)00504-5.

[3] V.A. Davankov, Chiral selectors with chelating properties in liquid chromatography: Fundamental reflections and selective review of recent developments, J. Chromatogr. A. 666 (1994) 55–76. https://doi.org/10.1016/0021-9673(94)80370-6.

[4] C.J. Welch, Evolution of chiral stationary phase design in the Pirkle laboratories, J. Chromatogr. A. 666 (1994) 3–26. https://doi.org/10.1016/0021-9673(94)80367-6.

[5] C. Fernandes, M.E. Tiritan, M. Pinto, Small Molecules as Chromatographic Tools for HPLC Enantiomeric Resolution: Pirkle-Type Chiral Stationary Phases Evolution, Chromatographia. 76 (2013) 871–897. https://doi.org/10.1007/s10337-013-2469-8.

[6] L.H. Easson, E. Stedman, Studies on the relationship between chemical constitution and physiological action, Biochem. J. 27 (1933) 1257–1266. https://doi.org/10.1042/bj0271257.

[7] C.E. Dalgliesh, 756. The optical resolution of aromatic amino-acids on paper chromatograms, J. Chem. Soc. Resumed. (1952) 3940. https://doi.org/10.1039/jr9520003940.

[8] A. Del Rio, J.M. Hayes, M. Stein, P. Piras, C. Roussel, Theoretical reassessment of Whelk-O1 as an enantioselective receptor for 1-(4-halogeno-phenyl)-1-ethylamine derivatives, Chirality. 16 (2004) S1–S11. https://doi.org/10.1002/chir.20009.

[9] C.F. Zhao, N.M. Cann, Molecular Dynamics Study of Chiral Recognition for the Whelk-O1 Chiral Stationary Phase, Anal. Chem. 80 (2008) 2426–2438. https://doi.org/10.1021/ac702126y.

[10] C.F. Zhao, S. Diemert, N.M. Cann, Rational optimization of the Whelk-O1 chiral stationary phase using molecular dynamics simulations, J. Chromatogr. A. 1216 (2009) 5968–5978. https://doi.org/10.1016/j.chroma.2009.06.041.

[11] M.E. Koscho, P.L. Spence, W.H. Pirkle, Chiral recognition in the solid state: crystallographically characterized diastereomeric co-crystals between a synthetic chiral selector (Whelk-O1) and a representative chiral analyte, Tetrahedron Asymmetry. 16 (2005) 3147–3153. https://doi.org/10.1016/j.tetasy.2005.08.027.

[12] B. Chankvetadze, Recent developments on polysaccharide-based chiral stationary phases for liquid-phase separation of enantiomers, J. Chromatogr. A. 1269 (2012) 26–51. https://doi.org/10.1016/j.chroma.2012.10.033.

[13] G.K.E. Scriba, Chiral recognition in separation sciences. Part I: Polysaccharide and cyclodextrin selectors, TrAC Trends Anal. Chem. 120 (2019) 115639. https://doi.org/10.1016/j.trac.2019.115639.

[14] J. Shen, Y. Okamoto, 8.11 Chromatographic Separations and Analysis: Cellulose and Polysaccharide Derivatives as Stationary Phases, in: Compr.

550   Chirality, Elsevier, 2012: pp. 200–226. https://doi.org/10.1016/B978-0-08-
551   095167-6.00824-7.
552 [15] G.K.E. Scriba, Chiral recognition in separation sciences. Part II: Macrocyclic
553   glycopeptide, donor-acceptor, ion-exchange, ligand-exchange and micellar
554   selectors, TrAC Trends Anal. Chem. 119 (2019) 115628.
555   https://doi.org/10.1016/j.trac.2019.115628.
556 [16] I. Ilisz, R. Berkecz, A. Péter, Retention mechanism of high-performance liquid
557   chromatographic enantioseparation on macrocyclic glycopeptide-based chiral
558   stationary phases, J. Chromatogr. A. 1216 (2009) 1845–1860.
559   https://doi.org/10.1016/j.chroma.2008.08.041.
560 [17] A. Berthod, 8.12 Chromatographic Separations and Analysis: Macrocyclic
561   Glycopeptide Chiral Stationary Phases, in: Compr. Chirality, Elsevier, 2012: pp.
562   227–262. https://doi.org/10.1016/B978-0-08-095167-6.00825-9.
563 [18] W.H. Pirkle, C.J. Welch, Use of simultaneous face to face and face to edge π-π
564   interactions to facilitate chiral recognition, Tetrahedron Asymmetry. 5 (1994)
565   777–780. https://doi.org/10.1016/S0957-4166(00)86225-4.
566 [19] E.R. Francotte, Enantioselective chromatography as a powerful alternative for
567   the preparation of drug enantiomers, J. Chromatogr. A. 906 (2001) 379–397.
568   https://doi.org/10.1016/S0021-9673(00)00951-1.
569 [20] E. Badaloni, W. Cabri, A. Ciogli, R. Deias, F. Gasparrini, F. Giorgi, A. Vigevani,
570   C. Villani, Combination of HPLC "Inverted Chirality Columns Approach" and
571   MS/MS Detection for Extreme Enantiomeric Excess Determination Even in
572   Absence of Reference Samples. Application to Camptothecin Derivatives, Anal.
573   Chem. 79 (2007) 6013–6019. https://doi.org/10.1021/ac070776j.
574 [21] E. Badaloni, W. Cabri, A. Ciogli, I. D'Acquarica, R. Deias, F. Gasparrini, F.
575   Giorgi, D. Kotoni, C. Villani, Extending the use of "Inverted Chirality Columns
576   Approach" for enantiomeric excess determination in absence of reference
577   samples: Application to a water-soluble camptothecin derivative, J. Chromatogr.
578   A. 1217 (2010) 1024–1032. https://doi.org/10.1016/j.chroma.2009.10.035.
579 [22] G. Mazzoccanti, O.H. Ismail, I. D'Acquarica, C. Villani, C. Manzo, M. Wilcox, A.
580   Cavazzini, F. Gasparrini, Cannabis through the looking glass: chemo- and
581   enantio-selective separation of phytocannabinoids by enantioselective ultra high
582   performance supercritical fluid chromatography, Chem. Commun. 53 (2017)
583   12262–12265. https://doi.org/10.1039/C7CC06999E.
584 [23] L. Sciascera, O. Ismail, A. Ciogli, D. Kotoni, A. Cavazzini, L. Botta, T. Szczerba,
585   J. Kocergin, C. Villani, F. Gasparrini, Expanding the potential of chiral
586   chromatography for high-throughput screening of large compound libraries by
587   means of sub–2µm Whelk-O 1 stationary phase in supercritical fluid conditions,
588   J. Chromatogr. A. 1383 (2015) 160–168.
589   https://doi.org/10.1016/j.chroma.2015.01.042.
590 [24] O.H. Ismail, G.L. Losacco, G. Mazzoccanti, A. Ciogli, C. Villani, M. Catani, L.
591   Pasti, S. Anderson, A. Cavazzini, F. Gasparrini, Unmatched Kinetic Performance
592   in Enantioselective Supercritical Fluid Chromatography by Combining Latest
593   Generation Whelk-O1 Chiral Stationary Phases with a Low-Dispersion in-House
594   Modified Equipment, Anal. Chem. 90 (2018) 10828–10836.
595   https://doi.org/10.1021/acs.analchem.8b01907.
596 [25] C.J. Welch, M. Biba, J.R. Gouker, G. Kath, P. Augustine, P. Hosek, Solving
597   multicomponent chiral separation challenges using a new SFC tandem column
598   screening tool, Chirality. 19 (2007) 184–189. https://doi.org/10.1002/chir.20357.

599 [26] E. Lesellier, C. West, The many faces of packed column supercritical fluid
600 chromatography - A critical review, J. Chromatogr. A. 1382 (2015) 2–46.
601 https://doi.org/10.1016/j.chroma.2014.12.083.
602 [27] C. West, Current trends in supercritical fluid chromatography, Anal. Bioanal.
603 Chem. 410 (2018) 6441–6457. https://doi.org/10.1007/s00216-018-1267-4.
604 [28] C. West, Enantioselective Separations with Supercritical Fluids - Review, Curr.
605 Anal. Chem. 10 (2014) 99–120. https://doi.org/10.2174/1573411011410010009.
606 [29] C. West, Recent trends in chiral supercritical fluid chromatography, TrAC Trends
607 Anal. Chem. 120 (2019) 115648. https://doi.org/10.1016/j.trac.2019.115648.
608 [30] S. Khater, M.-A. Lozac'h, I. Adam, E. Francotte, C. West, Comparison of liquid
609 and supercritical fluid chromatography mobile phases for enantioselective
610 separations on polysaccharide stationary phases, J. Chromatogr. A. 1467 (2016)
611 463–472. https://doi.org/10.1016/j.chroma.2016.06.060.
612 [31] R.W. Stringham, Relationship between resolution and analysis time in chiral
613 subcritical fluid chromatography, Chirality. 8 (1996) 249–257.
614 https://doi.org/10.1002/(SICI)1520-636X(1996)8:3<249::AID-CHIR4>3.0.CO;2-
615 C.
616 [32] C. West, Y. Zhang, L. Morin-Allory, Insights into chiral recognition mechanisms
617 in supercritical fluid chromatography. I. Non-enantiospecific interactions
618 contributing to the retention on tris-(3,5-dimethylphenylcarbamate) amylose and
619 cellulose stationary phases, J. Chromatogr. A. 1218 (2011) 2019–2032.
620 https://doi.org/10.1016/j.chroma.2010.11.084.
621 [33] C. West, G. Guenegou, Y. Zhang, L. Morin-Allory, Insights into chiral recognition
622 mechanisms in supercritical fluid chromatography. II. Factors contributing to
623 enantiomer separation on tris-(3,5-dimethylphenylcarbamate) of amylose and
624 cellulose stationary phases, J. Chromatogr. A. 1218 (2011) 2033–2057.
625 https://doi.org/10.1016/j.chroma.2010.11.085.
626 [34] S. Khater, Y. Zhang, C. West, Insights into chiral recognition mechanism in
627 supercritical fluid chromatography III. Non-halogenated polysaccharide
628 stationary phases, J. Chromatogr. A. 1363 (2014) 278–293.
629 https://doi.org/10.1016/j.chroma.2014.06.084.
630 [35] S. Khater, Y. Zhang, C. West, Insights into chiral recognition mechanism in
631 supercritical fluid chromatography IV. Chlorinated polysaccharide stationary
632 phases, J. Chromatogr. A. 1363 (2014) 294–310.
633 https://doi.org/10.1016/j.chroma.2014.06.026.
634 [36] S. Khater, C. West, Characterization of three macrocyclic glycopeptide
635 stationary phases in supercritical fluid chromatography, J. Chromatogr. A. 1604
636 (2019) 460485. https://doi.org/10.1016/j.chroma.2019.460485.
637 [37] A. Raimbault, C. West, Effects of high concentrations of mobile phase additives
638 on retention and separation mechanisms on a teicoplanin aglycone stationary
639 phase in supercritical fluid chromatography, J. Chromatogr. A. 1604 (2019)
640 460494. https://doi.org/10.1016/j.chroma.2019.460494.
641 [38] A. Raimbault, C.M.A. Ma, M. Ferri, S. Bäurer, P. Bonnet, S. Bourg, M.
642 Lämmerhofer, C. West, Cinchona-based zwitterionic stationary phases:
643 Exploring retention and enantioseparation mechanisms in supercritical fluid
644 chromatography with a fragmentation approach, J. Chromatogr. A. 1612 (2020)
645 460689. https://doi.org/10.1016/j.chroma.2019.460689.
646 [39] S. Khater, Y. Zhang, C. West, In-depth characterization of six cellulose tris-(3,5-
647 dimethylphenylcarbamate) chiral stationary phases in supercritical fluid

648   chromatography, J. Chromatogr. A. 1303 (2013) 83–93.
649   https://doi.org/10.1016/j.chroma.2013.06.040.

650 [40] C. West, E. Lemasson, S. Khater, E. Lesellier, An attempt to estimate ionic
651   interactions with phenyl and pentafluorophenyl stationary phases in supercritical
652   fluid chromatography, J. Chromatogr. A. 1412 (2015) 126–138.
653   https://doi.org/10.1016/j.chroma.2015.08.009.

654 [41] K.B. Lipkowitz, Theoretical studies of brush-type chiral stationary phases, J.
655   Chromatogr. A. 666 (1994) 493–503. https://doi.org/10.1016/0021-
656   9673(94)80411-7.

657 [42] R. Sheridan, W. Schafer, P. Piras, K. Zawatzky, E.C. Sherer, C. Roussel, C.J.
658   Welch, Toward structure-based predictive tools for the selection of chiral
659   stationary phases for the chromatographic separation of enantiomers, J.
660   Chromatogr. A. 1467 (2016) 206–213.
661   https://doi.org/10.1016/j.chroma.2016.05.066.

662 [43] W. Melander, J. Stoveken, C. Horváth, Stationary phase effects in reversed-
663   phase chromatography, J. Chromatogr. A. 199 (1980) 35–56.
664   https://doi.org/10.1016/S0021-9673(01)91360-3.

665 [44] R. Dallocchio, A. Dessì, M. Solinas, A. Arras, S. Cossu, E. Aubert, V. Mamane,
666   P. Peluso, Halogen bond in high-performance liquid chromatography
667   enantioseparations: Description, features and modelling, J. Chromatogr. A. 1563
668   (2018) 71–81. https://doi.org/10.1016/j.chroma.2018.05.061.

669 [45] W.F. Baitinger, P. von R. Schleyer, T.S.S.R. Murty, L. Robinson, Nitro groups as
670   proton acceptors in hydrogen bonding, Tetrahedron. 20 (1964) 1635–1647.
671   https://doi.org/10.1016/S0040-4020(01)99161-6.

672 [46] M.E. Koscho, W.H. Pirkle, Investigation of a broadly applicable chiral selector
673   used in enantioselective chromatography (Whelk-O 1) as a chiral solvating agent
674   for NMR determination of enantiomeric composition, Tetrahedron Asymmetry.
675   16 (2005) 3345–3351. https://doi.org/10.1016/j.tetasy.2005.08.032.

676 [47] A. Knežević, J. Novak, V. Vinković, New Brush-Type Chiral Stationary Phases
677   for Enantioseparation of Pharmaceutical Drugs, Molecules. 24 (2019) 823.
678   https://doi.org/10.3390/molecules24040823.

679 [48] P. Gamez, T.J. Mooibroek, S.J. Teat, J. Reedijk, Anion Binding Involving π-
680   Acidic Heteroaromatic Rings, Acc. Chem. Res. 40 (2007) 435–444.
681   https://doi.org/10.1021/ar7000099.

682 [49] M. Lämmerhofer, Chiral recognition by enantioselective liquid chromatography:
683   Mechanisms and modern chiral stationary phases, J. Chromatogr. A. 1217
684   (2010) 814–856. https://doi.org/10.1016/j.chroma.2009.10.022.
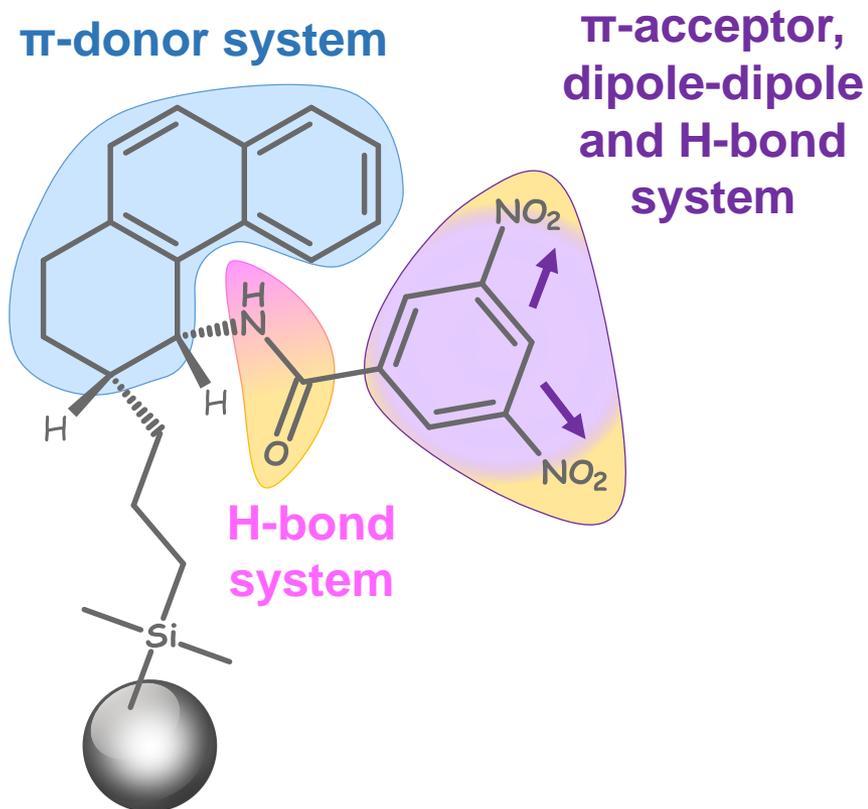
685

Figure 1. Structure of the chiral selector in the (R,R)-Whelk-O1 stationary phase and features of the different fragments of the chiral selector. The ligand in ReproSil Chiral-NR is the (S,S) enantiomer of this one.
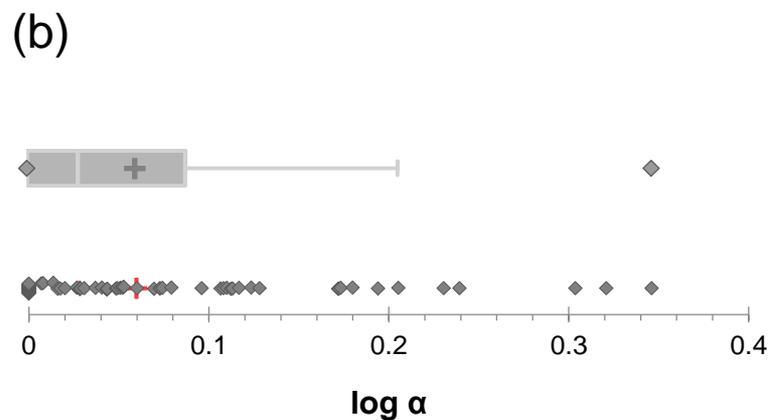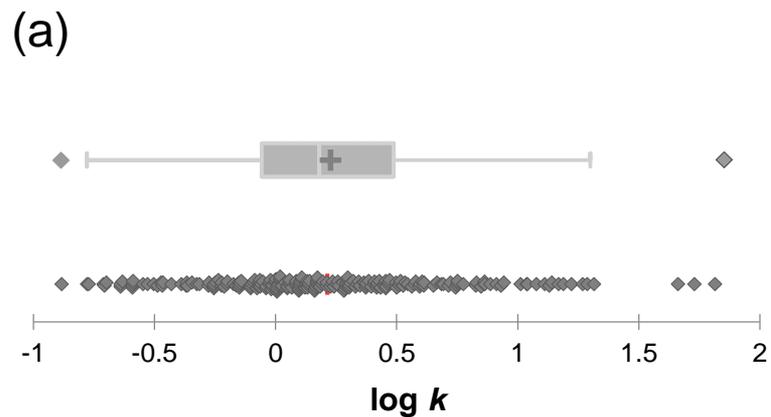
Figure 2. Scattergrams and box-plots of (a) retention factors for the 212 achiral analytes in Table S1 and (b) separation factors for the 79 racemates in Table S2 on (R,R)-Whelk-O1. Chromatographic conditions: CO_2-methanol 90:10 (v/v), 25°C, 15 MPa, 3 mL/min.
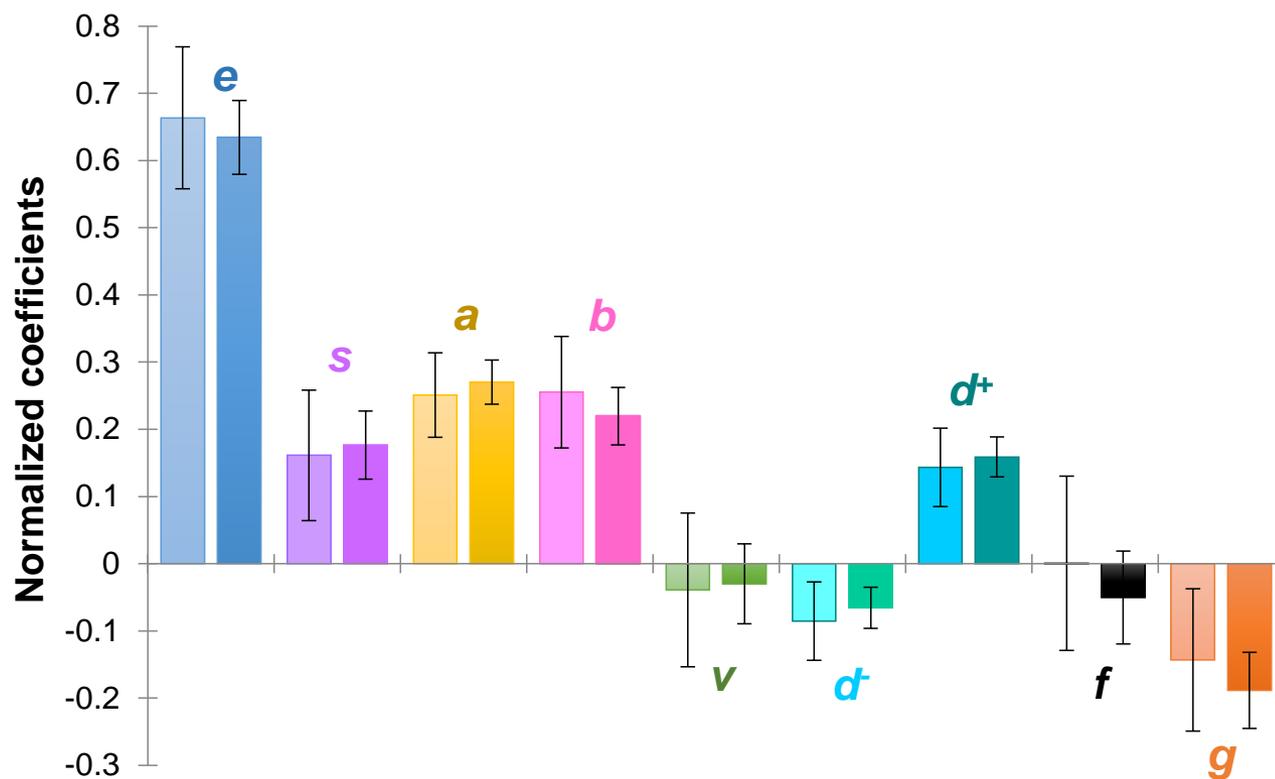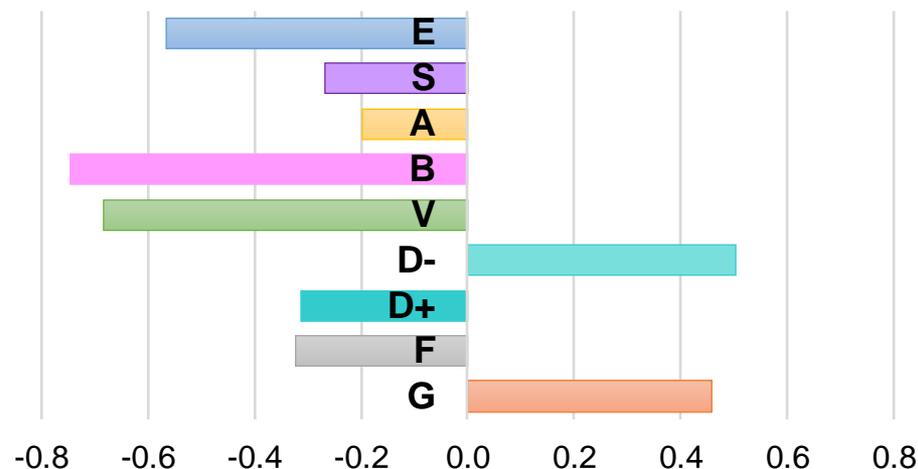
Figure 3. Histogram representing normalized coefficients of the LSER model calculated with the retention data measured for the 212 analytes in Table S1 and Eq. (1) on the (R,R)-Whelk-O1 column (left bars) and ReproSil Chiral-NR column (right bars). Error bars indicate the 95% confidence limits. Chromatographic conditions: see Figure 2.

Figure 4. Discriminant analyses using nine molecular descriptors as variables and the 79 racemates eluted from (R,R)-Whelk-O1 in Table S2.
(a) Discrimination between early-eluting (left) and late-eluting (right) racemates indicating the structural features favouring some form of exclusion from the stationary phase (left) or inclusion (right).
(b) & (c) Discrimination between non-separated (left) and separated (right) racemates where negative features are common to the racemates that were not separated on this stationary phase and positive features are common to separated racemates. (b) including all racemates (c) including only early-eluting racemates.
Chromatographic conditions: see Figure 2.

Figure 5. Bubble graphs to compare retention and separation values for the chiral analytes in Table S2 depending on their structural features. Large bubbles indicate large values for each molecular descriptor.
Chromatographic conditions : see Figure 2.

Figure 1: Structure of the chiral selector in the (R,R)-Whelk-O1 stationary phase and features of the different fragments of the chiral selector. The ligand in ReproSil Chiral-NR is the (S,S) enantiomer of this one.

Figure 2: Scattergrams and box-plots of (a) retention factors for the 212 achiral analytes in Table S1 and (b) separation factors for the 79 racemates in Table S2 on (R,R)-Whelk-O1. Chromatographic conditions: CO_2-methanol 90:10 (v/v), 25°C, 15 MPa, 3 mL/min.

Figure 3: Histogram representing normalized coefficients of the LSER model calculated with the retention data measured for the 212 analytes in Table S1 and Eq. (1) on the Whelk-O1 column (left bars) and Reprosil Chiral-NR column (right bars). Error bars indicate the 95% confidence limits. Chromatographic conditions: see Figure 2.

Figure 4: Discriminant analyses using nine molecular descriptors as variables and the 79 racemates eluted from (R,R)-Whelk-O1 in Table S2.

(a) Discrimination between early-eluting (left) and late-eluting (right) racemates indicating the structural features favouring some form of exclusion from the stationary phase (left) or inclusion (right).

(b) & (c) Discrimination between non-separated (left) and separated (right) racemates where negative features are common to the racemates that were not separated on this stationary phase and positive features are common to separated racemates. (b) including all racemates (c) including only early-eluting racemates.
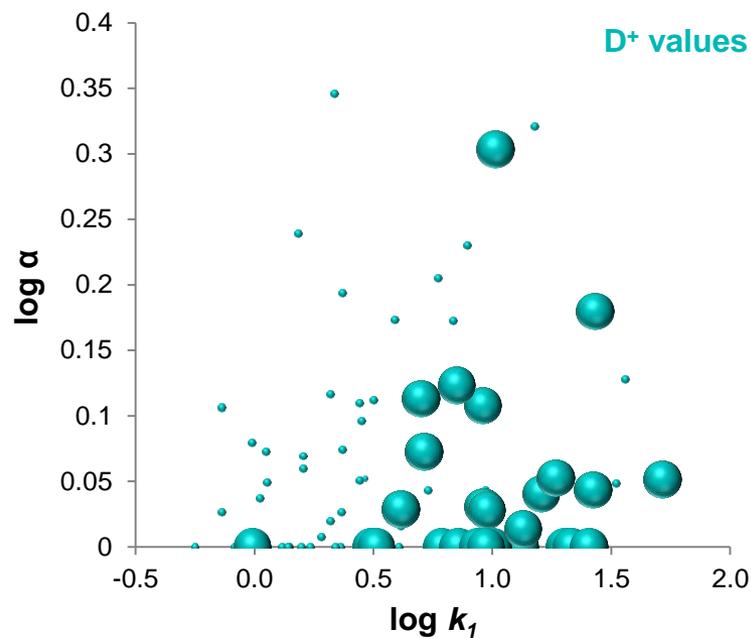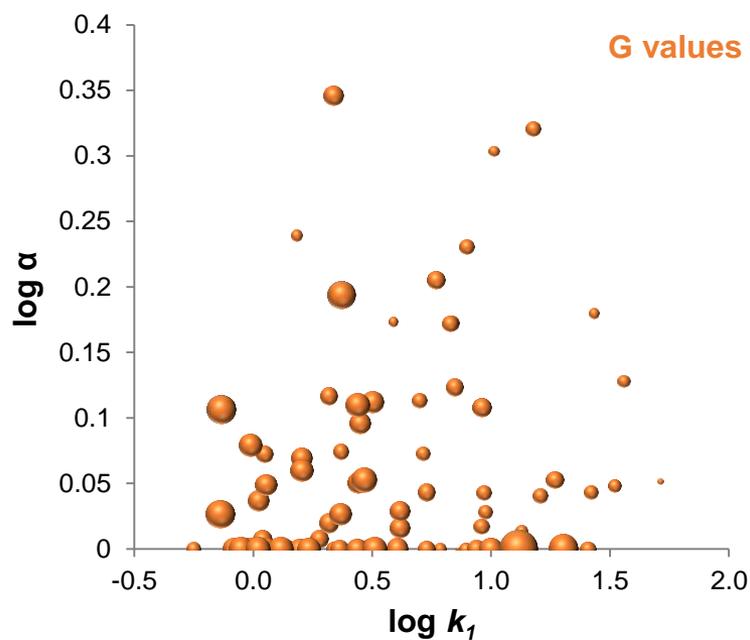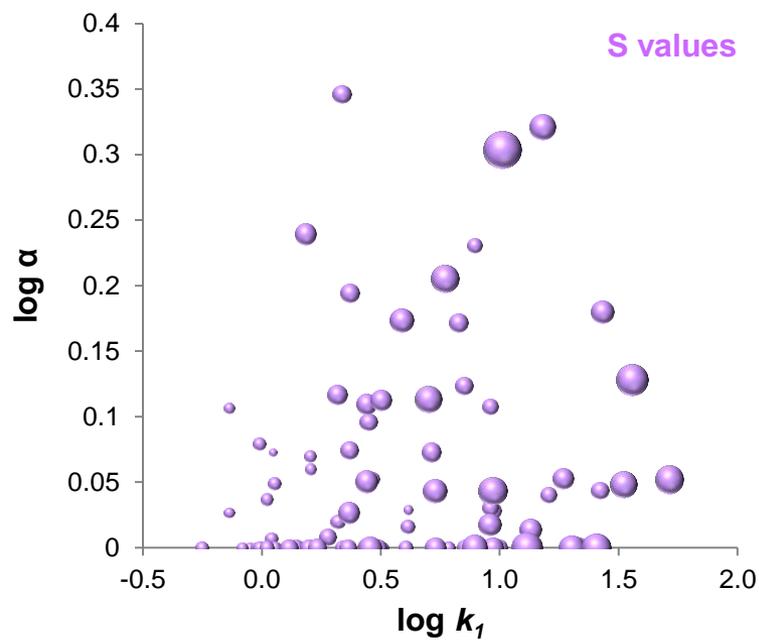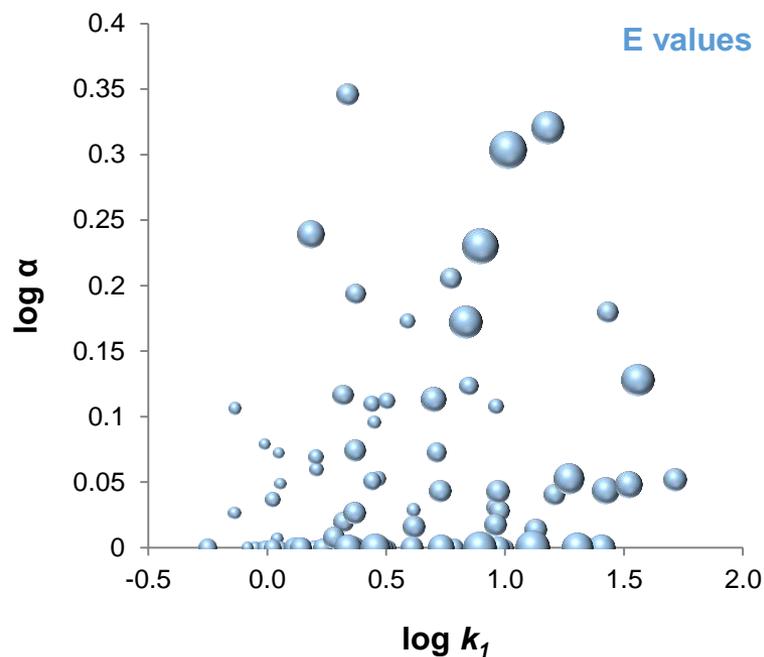
Figure 5: Bubble graphs to compare retention and separation values for the chiral analytes in Table S2 depending on their structural features. Large bubbles indicate large values for each molecular descriptor.

Table 1 system constants and statistics for the 2 columns tested
obtained with Eq.(1), with or without additive in the mobile phase
n is the number of solutes finally retained in the multiple linear regression;
R^2_{adj} is the adjusted determination coefficient; *SE* in the standard error in the estimate

Column	*c*	*e*	*s*	*a*	*b*	*v*	*d⁻*	*d⁺*	*f*	*g*	n	R^2_{adj}	*SE*
Whelk-O1	-0.640	0.598	0.184	0.361	0.413	-0.039	-0.137	0.258	0.000	-0.190	212	0.856	0.280
	0.167	*0.048*	*0.056*	*0.046*	*0.068*	*0.058*	*0.047*	*0.053*	*0.036*	*0.071*			
ReproSil Chiral-NR	-0.413	0.462	0.159	0.307	0.284	-0.024	-0.081	0.259	-0.021	-0.195	200	0.854	0.142
	0.136	*0.040*	*0.045*	*0.037*	*0.055*	*0.047*	*0.038*	*0.049*	*0.030*	*0.058*			